ACS OMEGA

http://pubs.acs.org/journal/acsodf

Article

Gold Nanorod-Induced Effects in a Mesogenic Compound 4-(*trans*-4-*n*-Hexylcyclohexyl) isothiocyanatobenzene

Abhinav Lal,* Himanshu Verma, Saikumar Chirra, Ravindra Dhar,* Roman Dabrowski, and Kusum Lata Pandey

Cite This: *ACS Omega* 2023, 8, 29012−29024

Read Online

ACCESS | Metrics & More | Article Recommendations

ABSTRACT: Gold nanorods (GNRs) have a capsule-like structure with different optical properties than spherical gold nanoparticles due to surface plasmon resonance. Liquid crystals (LCs) are mesogenic compounds having crystal-like orientation and liquid-like fluidity. They are important materials from a technological point of view. Both GNRs and LC compounds are anisotropic in shape and properties. Different nano entities show interesting results when dispersed in different liquid crystalline materials which are instrumental from the application point of view. In the present work, GNRs have been dispersed in nematic liquid crystalline materials, namely 4-(*trans*-4-*n*-hexylcyclohexyl) isothiocyanatobenzene (6CHBT). Calorimetric, texture, spectroscopic, and dielectric studies were carried out for a pure 6CHBT and its composites with GNRs. Different calorimetric and dielectric parameters such as transition temperature, enthalpy, heat flow, permittivity, dielectric strength, dielectric anisotropy, and relaxation frequency have been determined, and the effect of GNRs has been explored. This article gives an insight into the influence of GNRs on the morphology and anisotropic physical properties of the nematic liquid crystalline material.

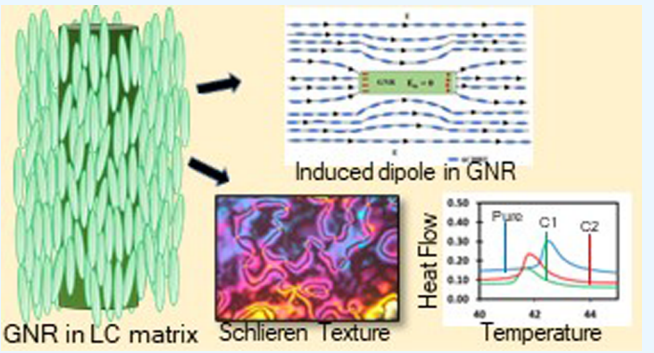

1. INTRODUCTION

The study of new and advanced materials is carried on extensively to meet various technological, energy, and economic needs. One such material is a liquid crystal (LC). They are mesogenic molecules that show a counterintuitive combination of fluidity and long-range order. Due to this, they show various properties intermediate to that of crystalline solids and isotropic liquids. Although LCs are not new to this area of research but studies on them are going on broadly in the field of synthesis of new LC materials, their characterization, and preparation of composites by addition of different kinds of dopants to meet certain applicative needs. LCs find their application in the field of display technology, optics, electro-optics, bioscience, biophotonics, actuators, etc. These applications are due to their structural, orientational, transitional, thermal, dielectric, and optical properties.[1,2] LCs are majorly classified on the basis of the driving force for their existence as mesogenic molecules, namely thermotropic, lyotropic, and metallotropic. Thermotropic LCs are the most widely studied LC due to the existence of their mesogenic properties on temperature change. They are further classified into calamitic and discotic on the basis of the structure and orientation of molecules. In the case of calamitic LCs, the overall length of the molecule is significantly greater than its width.[3,4] The most common phase used in various applications shown by the calamitic LCs is the nematic phase. The nematic phase is the least ordered where no translational but only orientational order is present.[5,6] As far as stereochemistry is concerned, nematic LC is symmetrical with the C_α axis along the director with the $D_\alpha h$ point group. Materials with a size range of 2−100 nm are known as nanomaterials. They vary in shape depending upon the material of which it is prepared and also on the type of method by which they are prepared. As the shape varies, their physical property will also vary. Nanorods come under 1D nanomaterials along with nanotubes and nanowires. Nanorods have no internal surface in comparison to nanotubes whereas in comparison to nanowires, the length of nanowires is considerably larger than in nanorods.[7]

Various research reveals that nanomaterials play an important role in altering and improving the properties of LC molecules. A large number of LC-nanomaterial composites

Received: March 20, 2023
Accepted: July 21, 2023
Published: August 3, 2023

have been prepared and studied extensively to understand the effect of nanomaterials on the physical and chemical properties of LCs.[3,8−16] Dopants like quantum dots of CdSe, carbon, nanoparticles of $BaTiO_3$, silver, gold, MgO, and single and multiwall carbon nanotubes were used.[17,18] Paul et al. doped 0.5 wt % $BaTiO_3$ nanopowder in 6CHBT which led to a decrease in I−N transition and enthalpy value.[19] Tripathi et al. doped 0.6 wt % Silver nanoparticles of 5 and 100 nm size in 6CHBT LC and observed a nominal increase in I−N transition temperature and marginal decrease in dielectric anisotropy.[9] Patro et al. doped 0.04 wt % COOH-functionalized multiwall carbon nanotube in 6CHBT which results in an increase of N−I transition temperature, average transition enthalpy, and entropy. For this composite, the value of dielectric anisotropy decreased, whereas relaxation frequency increased.[20] It has also been studied and reported that the concentration and size of nanomaterials used for doping play a major role in the stability of mesophases. Concentration less than 1 weight percent and size in the range of 10−50 nm is favorable.[21] If any of these factors or both increases, they induce elastic distortion on the director of LC molecules.[22,23] Several literature studies also reveal that on addition of nanomaterials, ordering in LC molecules has increased and it has favored several parameters to improve different applications. It is also observed that those composite systems which have either rod-like nanomaterials like SWCNT, MWCNT, etc., or gold nanoparticle has shown a positive sign in nematic ordering.[24−26] Not only nanomaterials alter the properties of LCs but there are several properties of nanomaterials that get altered when they are introduced into the surrounding of LC molecules.[27−29]

Most of the studies have been carried out using spherical nanoparticles, carbon nanotubes, quantum dots, etc. Nanorods that have anisotropic shapes and properties like those of LCs are less studied. GNRs are capsule-like nanomaterials with a size of a few nanometers to hundreds of nanometers. They show a property of difference in polarization of electrons along the short-axis and long-axis direction. Their absorption spectra show two peaks, one in the visible region due to polarization of electrons along the short axis and the other in the visible or near IR region due to polarization along the long axis.[8,30,31]

Hence, in the present work, we have dispersed GNRs in a nematic LC (NLC) material namely 4-(*trans*-4-*n*-hexylcyclohexyl)isothiocyanatobenzene (6CHBT).[19] Its molecular formula is $C_{19}H_{27}NS$ and its molecular weight is 301.5 g/mol. It has low viscosity and high chemical stability, and it is polar in nature due to the presence of a highly negative NCS group which results in its dipole moment value of 3.5 D.[32] It is a room-temperature nematic which has a nematic phase range from 11.5 to 42.5 °C. The GNRs used here have a varying length of 46−56 nm and a diameter of 9−15 nm. Considering the average value of length (51 nm) and diameter (12 nm), the aspect ratio which is length divided by width is obtained to be 4.25.

The key objective of this work is to understand the interaction of a rod-shaped nanomaterial with rod-like NLC molecules, to understand how GNR interacts with or affects the molecular arrangement of NLC, and also, to study the effect of GNRs on calorimetric, texture, dielectric, and spectroscopic properties of mesogenic 6CHBT. Through these studies, the stability of different phases and compound as a whole of LC molecules can also be understood.

2. EXPERIMENTAL TECHNIQUES

2.1. Materials. 6CHBT NLC was synthesized and purified at the Military University of Technology, Warsaw, Poland. Its chemical structure is shown in Figure 1. It shows Cr−N

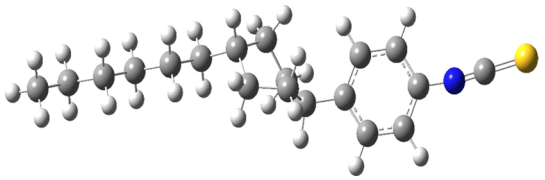

Figure 1. Molecular structure of 4-(*trans*-4-*n*-hexylcyclohexyl) isothiocyanatobenzene (6CHBT).

transition at 11.5 °C and N−I transition at 42.5 °C.[10,24] The DSC thermogram along with POM-derived textures for its pure form is shown in Figure 2. GNR was procured from Alfa Aesar having a dimension of 9−15 nm diameter and 46−56 nm length. It is dispersed in water, and the concentration is 100 ± 1 mg in 1000 mL water.

2.2. Preparation of Composites. The 6CHBT-GNR composites were prepared in two different concentrations. Composite 1 is prepared by dispersing 0.05 wt % GNRs in pure 6CHBT LC, whereas composite 2 is prepared by dispersing 0.1 wt % GNRs in pure 6CHBT. Chloroform was used as a solvent for the preparation of composites. To achieve 0.05 wt % concentration, 0.27 mL (270 μL) of GNRs dispersed in water was mixed with 2 mL chloroform with 6CHBT. For 0.1 wt % concentration, 0.54 mL (540 μL) of GNRs dispersed in water was mixed with 2 mL chloroform with 6CHBT. For uniform dispersion of GNRs in 6CHBT medium, the mixture was ultrasonicated for about 2 h. After this, the composite mixture was left in a dry atmosphere for complete evaporation of chloroform and water contents from the mixture. Perfect removal of chloroform and water was checked through dielectric measurements discussed in Section 3.4. All the weighing was performed using semimicro balance by Shimadzu (AUW120D). A calorimetric study of a pure 6CHBT sample and its composites were carried out using a Differential Scanning Calorimeter (DSC) by NETSZCH (DSC-200-F3-Maia). A sample of weight approximately 3 mg was weighed and sealed in an aluminum pan. The sealed pan was kept inside the sample holder. The endothermic and exothermic cycle was run for 2 complete cycles from −20 to 60 °C to stabilize the value of transition temperature and enthalpies of transition. The heating and cooling cycles were performed at the scan rate of 2.5, 5.0, 7.5, 10.0, 12.5, and 15.0 °C/min out of which the values of scan rate 5 °C/min are reported here. With the increase of scan rate, the transition temperature for nematic isotropic transition increases for heating cycle, whereas it decreases for cooling cycle.[20] Extrapolated transition temperatures at the (hypothetical) scan rate of 0 °C/min are supposed to be true transition temperatures under thermal equilibrium. Although a low scan rate is more appropriate (due to being close to thermal equilibrium), sometimes weak transition peaks are flattened and hence missed. On the contrary, fast scan rates keep the transition process away from thermal equilibrium. For these reasons, a scan rate of 5 °C/min is supposed to be the optimum rate and displayed here in typical plots. Moreso, DSC has been calibrated at the scan rate of 5 °C/min keeping the above points in mind. The data analysis was performed using

https://doi.org/10.1021/acsomega.3c01863
ACS Omega 2023, 8, 29012−29024

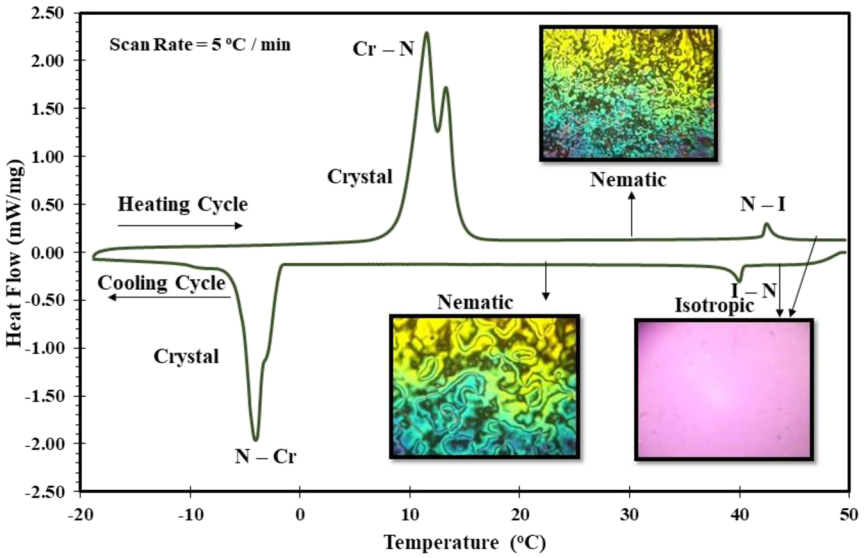

Figure 2. DSC thermogram and optical textures of pure 6CHBT for both heating and cooling cycle showing Cr–N and N–I transitions.

Table 1. Peak Transition Temperatures (T_p in °C), Width of Transition (ΔT in °C), Enthalpy of Transition (J/g) for Pure 6CHBT NLC, and Its Composites with GNRs at a Scan Rate of 5°/min

	heating cycle			cooling cycle		
	N–I transition			I–N transition		
	T_p (°C)	ΔT (°C)	ΔH (J/g)	T_p (°C)	ΔT (°C)	ΔH (J/g)
pure 6CHBT	42.5	0.8	0.14	41.4	0.9	0.15
6CHBT + 0.05 wt % GNRs	41.7	1.0	0.08	40.7	1.1	0.09
6CHBT + 0.1 wt % GNRs	41.8	0.9	0.12	40.9	1.0	0.14

Proteus Analysis Software provided by NETZSCH. The dielectric study was performed in an Impedance Analyzer of NOVO Control, Germany (Model Alpha A-Analyzer) in the frequency range of 1 Hz–10 MHz. Dielectric data were recorded in a cooling cycle at the rate of 0.2 °C/min with a measuring electric field of 0.5 V_{rms}. Temperature of the sample during the dielectric measurement was controlled by a hot stage from Instec (Model HS-1) with an accuracy of ±0.1 °C and a temperature resolution of 3 mK. To attain planar alignment of the molecules (to measure transverse–perpendicular component of the permittivity), ITO glass plates were rubbed unidirectionally with a polyimide layer and spacers of thickness 10 μ was used. Similarly, for the homeotropic alignment of the molecules (to measure the longitudinal–parallel component of the permittivity), ITO glass plates were coated with lecithin and separated by mylar spacers of 10 μ thickness. The texture studies were carried out with the help of a Polarizing Optical Microscope by Central Scientific Instrument Corporation (CENSICO), Agra, India, attached with a still camera to capture the image. The pure and composite samples were taken in between glass slide and cover slip (unaligned molecules) and placed under a polarized optical microscope and observations were made in the dark state. Optical textures were recorded in the cooling cycle at 0.2 K/min scan rate. FTIR studies were carried out in a Perkin Elmer Spectrum 2 spectrophotometer using KBr plates in the wave number range of 4000–400 cm^{-1}.

3. RESULTS AND DISCUSSION

3.1. Calorimetric Study—Transition Temperature and Enthalpy. The calorimetric data of pure 6CHBT and its GNR composites were obtained and certain variations in the value of transition temperature and enthalpy change are observed. The transition temperature for the nematic to isotropic (N–I) transition decreased for composite 1 (0.05 wt % GNRs in 6CHBT) from 42.5 °C of pure 6CHBT to 41.7 °C as can be seen in Table 1. When this nanorod concentration was raised to 0.1 wt % of GNRs in composite 2, the value of nematic to isotropic transition slightly increased (41.8 °C), but it is still less than that of pure 6CHBT. However, for the crystal-to-nematic (Cr–N) transition, the value of transition temperature for composite 1 increases from 11.5 °C of pure 6CHBT to 12.9 °C. For composite 2, the value further increases to 13 °C. Figure 3 shows a comparative DSC thermogram of pure 6CHBT and their GNR composites in the heating and cooling cycle.

A decrease in N–I transition temperature on the addition of nanomaterials can be very well understood by mean-field theory given by Gorkunov and Osipov.[33] The major assumption of this theory is that the concentration of nanomaterials doped is very small which nullifies their self-interaction. Also, the shape should be nonspherical and the size of nanomaterials, particularly diameter, should be sufficiently larger than the length of mesogenic molecules so that the interaction between the nanomaterial and mesogenic molecules is through the surface only. In our system, the nanomaterial used is GNR whose diameter is in the range of 9–15 nm, whereas the size of our LC molecule is around 2 nm.[34] According to Gorkunov and Osipov, the transition temperature (T'_{NI}) of the nanomaterial-LC mixture is a function of an anisotropic nanomaterial as

https://doi.org/10.1021/acsomega.3c01863
ACS Omega 2023, 8, 29012–29024

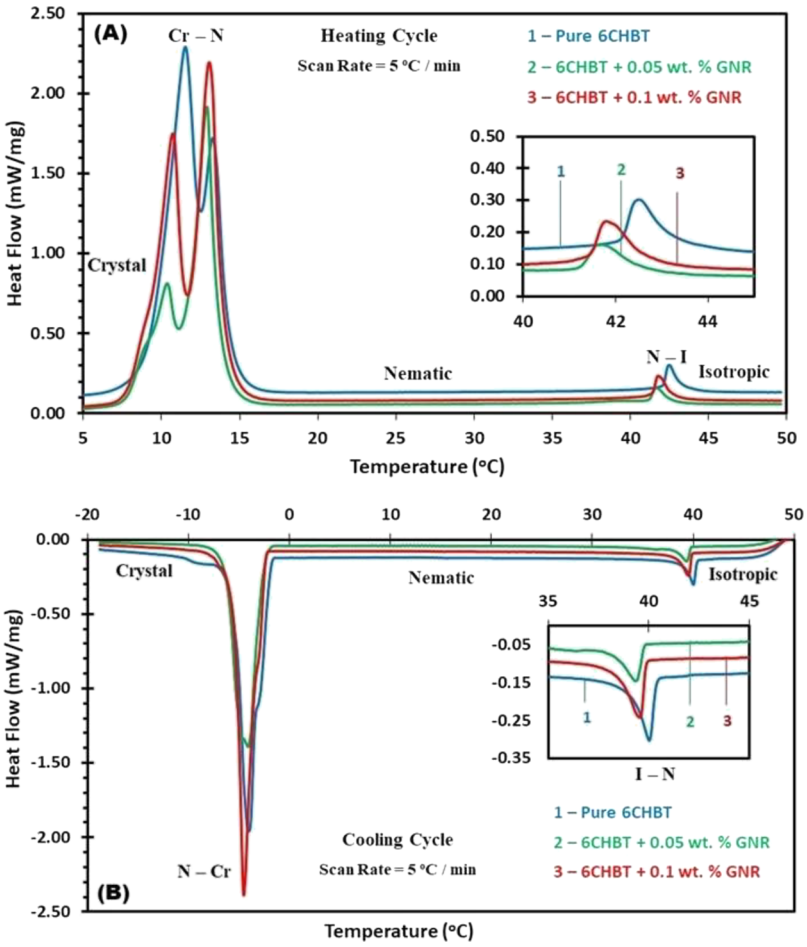

Figure 3. DSC thermogram of pure 6CHBT (Curve 1), composite 1 (Curve 2), and composite 2 (Curve 3) for heating cycle (A) and cooling cycle (B).

$$T'_{NI} \approx T_{NI}(1-\nu)\left[1+\nu\frac{2W^2}{15|w|k_B T_0 \nu_p}\right] \quad (1)$$

where T_{NI} is the transition temperature of the host without the nanomaterial, ν is the volume fraction of the dispersed nanomaterial in the mixture, ν_p is the average volume of the dispersed nanomaterial, and k_B is Boltzmann's constant. W and w are the coupling constants between the LC-nanomaterial system and LC-LC molecules, respectively. When the concentration of the nanomaterial is very low, then the square bracket term of eq 1 turns to be 1. Hence, eq 1 becomes $T'_{NI} \approx T_{NI}(1-\nu)$. The variation of T'_{NI} can be understood by two mechanisms. First, due to the presence of nanomaterial, the average separation between the LC molecule in the LC matrix increases. This is considered as a "dilution" effect. Due to an increase in separation between LC molecules, the strength of intermolecular interaction decreases which reduces the nematic ordering resulting in the decrease of value of transition temperature. The reduction of the nematic ordering is supported by the enthalpy (ΔH) change observed for this transition. The value of ΔH decreases from 0.14 J/g for pure to 0.08 J/g for composite 1 with 0.05 wt % GNRs.[35] Mishra et al. have also suggested that upon the addition of GNPs, the average bonding strength is decreased which was evident from the decrease of values of ΔH.[36] The second mechanism suggests that the nanomaterial gets partially aligned along the LC director leading to better nematic ordering. Kopcansky et al. have also suggested that when the shape of nanomaterial is rod-like then rigid anchoring is observed.[37] As the ordering is improved, the transition temperature increases. This is also visible from eq 1 through the term containing W. With the increase of interaction between the nanomaterial and LC molecules, W increases which results in the increase of T'_{NI}. For a nanomaterial−LC mixture at a certain concentration, this effect compensates the negative "dilution" effect leading to constant values of thermodynamic parameters. In our second composite, when the concentration of GNRs is increased to 0.1 wt %, the transition temperature is increasing which is due to the second mechanism explained in Mean-Field theory. This is in agreement with the increase in the value of enthalpy change for N−I transition for composite 2 (0.12 J/g). This interaction of GNRs and LC molecules will be further discussed in the forthcoming section of the dielectric study. An approximate calculation of the ratio of LC molecules with GNRs was carried out and found to be 1300:1 for composite 1 and 650:1 for composite 2. It shows that with a doubling of GNR concentration, the number of LC molecules per GNR becomes half. With the increase of GNR, the LC-GNR interaction enhances and nematic ordering dominates the dilution effect. Hence, the value of T'_{NI} starts to increase. The same has been observed in our studies as evident from Table 1. Figure 3A shows double peaks during the melt process which are represented as Cr−Cr′ and Cr′−N transitions. Two peaks appear due to initial melt with simultaneous partial

https://doi.org/10.1021/acsomega.3c01863
ACS Omega 2023, 8, 29012−29024

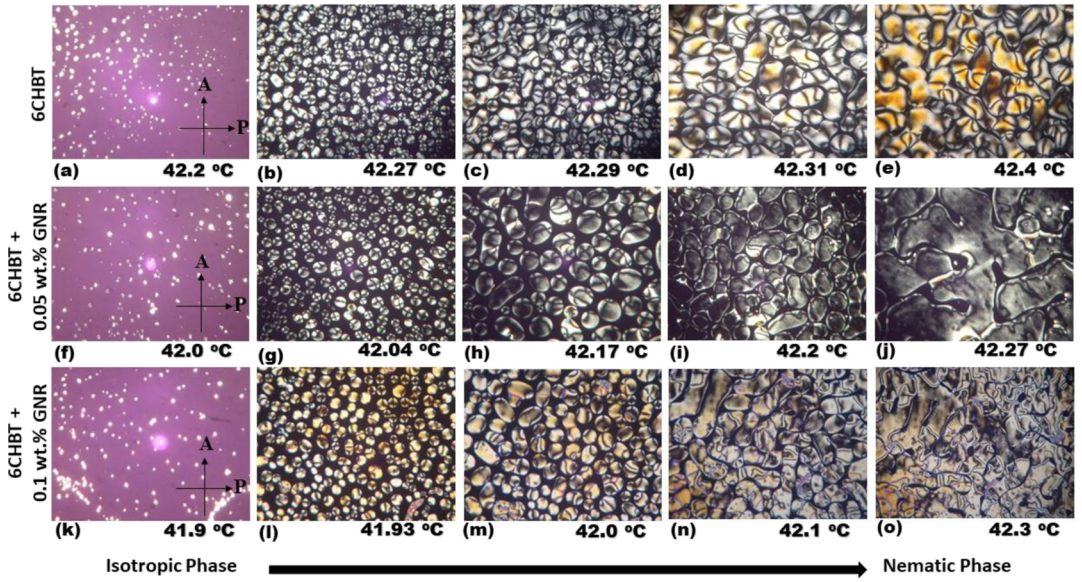

Figure 4. POM image showing growth of nematic droplets during I−N transition for pure 6CHBT (a−e); 6CHBT + 0.05 wt % GNRs (f−j) and 6CHBT + 0.1 wt % GNRs (k−o). Samples were taken in between the glass slide and cover slip (unaligned molecules).

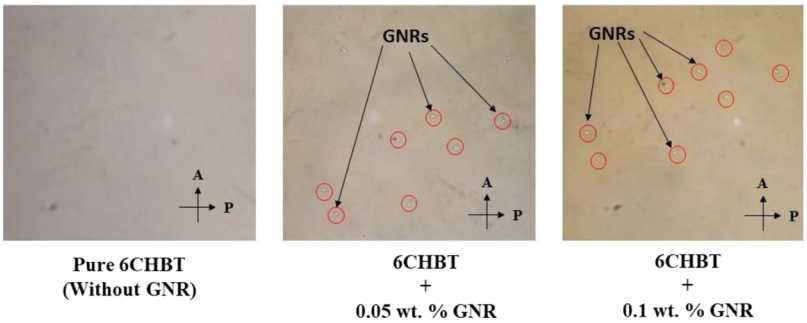

Figure 5. POM image (magnification 150×) showing the distribution of GNRs in pure 6CHBT in the nematic phase in a planar-aligned cell.

recrystallization (making it a mixed crystal state Cr′) and then complete melt from Cr′ to nematic phase.[3,21,38,39] Witko et al. have suggested that the structural complexity in bulk 6CHBT is the reason for such a double melt (and sometimes during crystallization too) visible in DSC thermograms.[40]

3.2. Texture Study—Droplet Morphology of NLCs. A texture study was performed to confirm the different phases and distribution of GNRs in the LC medium. The isotropic to nematic phase transition was observed by the formation of droplets that are closely packed in a specific orientation. With the decrease of temperature, each droplet binds with neighboring droplets such that deformation of a spherical shape is observed which later on results in the formation of bigger droplets and ultimately leads to the formation of a nematic layer. This study was performed for pure 6CHBT and its composites with GNRs where a similar kind of droplet formation takes place but at different temperature ranges. Figure 4 shows the formation of droplets at the isotropic−nematic transition in cooling cycle at a specific temperature. It is observed that on addition of 0.05 wt % of GNRs, the alignment of LC molecules has decreased (i and j in Figure 4). It occurs due to a decrease in intermolecular interaction resulting in a decrease of nematic ordering which is explained in the calorimetric study by Mean-Field theory. However, in composite 2, the concentration of GNRs is increased, due to which crowding of molecules takes place. Due to these crowding, molecules try to align themselves in a given volume which results in a better nematic layer (n and o in Figure 4) than in composite 1. This is also evident from calorimetric data and reason explained through Mean-field theory. The texture study of planar-aligned samples confirms the presence of GNRs (Figure 5). For planar-aligned samples, the nematic phase of pure 6CHBT does not show any bright spots, but the nematic phase of both the composites shows white spots due to the presence of GNRs. These white spots are observed due to the birefringence of GNRs.[29,41]

3.3. FTIR Spectroscopic Study. Fourier transform infrared spectroscopic studies were performed to understand the effect of addition of GNRs on the type of bonding in the host 6CHBT molecule. FTIR spectra of pure 6CHBT and their composites with GNRs consist of several peaks in the range of 3000−500 cm^{-1} (Figure 6) The following peaks are observed at 2922, 2852, 2080, 1505, 1447, 934, 829, and 537 cm^{-1} for pure 6CHBT. The peak at 2922 cm^{-1} occurs due to asymmetric stretching of the C−H_2 groups ($\nu_{as}^{CH_2}$). The peak at 2852 cm^{-1} is due to symmetric stretching of CH_2 groups ($\nu_{s}^{CH_2}$). The peak at 2080 cm^{-1} is due to asymmetric stretching of the −NCS group (ν_{as}^{NCS}). The peak observed at 1505 cm^{-1} is related to the aromatic ring which contracts C−C bonds in the aromatic ring and rocking in-plane bending of aromatic hydrogen atoms in the plane of the aromatic ring ($\nu_{as}^{(C=C)}$). The peak observed at 1447 cm^{-1} is due to scissor-

https://doi.org/10.1021/acsomega.3c01863
ACS Omega 2023, 8, 29012−29024

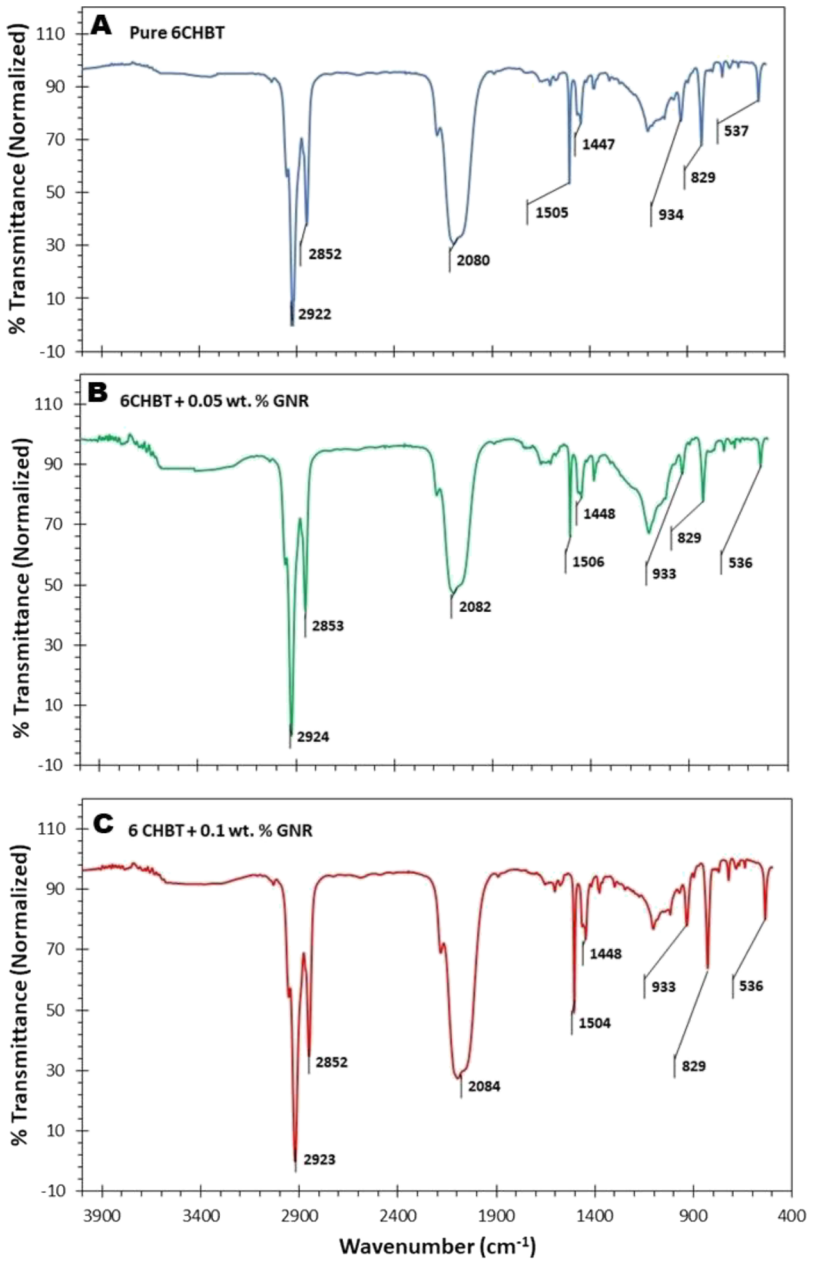

Figure 6. FTIR spectra of percentage transmittance versus wavenumber (cm^{-1}) for pure 6CHBT (A), composite 1 (B), and composite 2 (C) showing normalized peaks.

Table 2. Value of Wavenumber in cm^{-1} of Various Peaks Occurred in FTIR Spectra of Pure 6CHBT and its Composites with GNRs (from Figure 6)

		wave number (cm^{-1})		
s. no.	type of vibrations	pure 6CHBT	6CHBT + 0.05 wt % GNRs	6CHBT + 0.1 wt % GNRs
1	($\nu_{as}^{CH_2}$)	2922	2924	2923
2	($\nu_{s}^{CH_2}$)	2852	2853	2852
3	(ν_{as}^{NCS})	2080	2082	2084
4	($\nu_{as}^{\text{benzene ring}}$)	1505	1506	1504
5	($\delta_{s}^{CH_2}$)	1447	1448	1448
6	out of plane	934	933	933
7	($\gamma^{(=CH)}$)	829	829	829
8	(δ^{NCS}) or ($\gamma^{(=CH)}$)	537	536	536

type in-plane bending of $-CH_2$ group ($\delta_{s}^{CH_2}$). The peak at 829 cm^{-1} occurs due to out-of-plane bending of aromatic hydrogen atoms ($\gamma^{(=CH)}$). The peak at 537 cm^{-1} is may be due to either in-plane bending of the NCS group or out-of-plane bending of

https://doi.org/10.1021/acsomega.3c01863
ACS Omega 2023, 8, 29012−29024

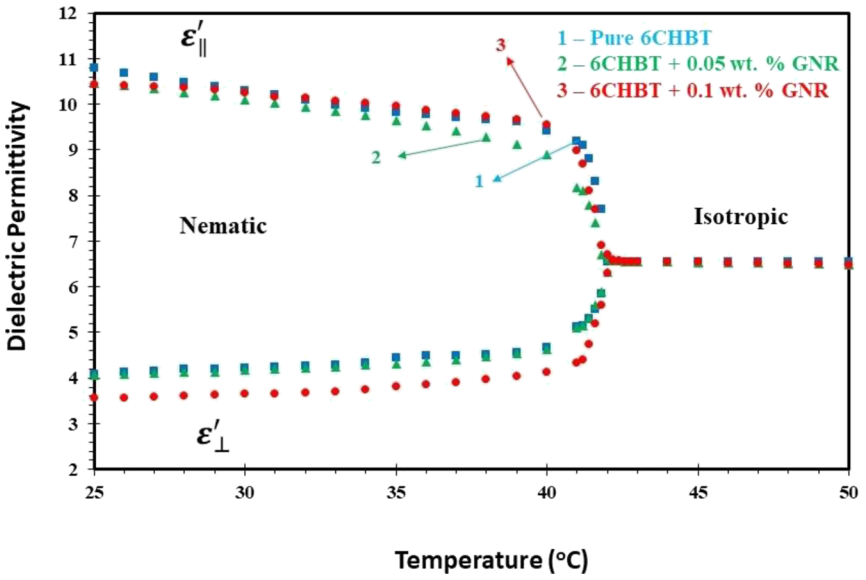

Figure 7. Variation of the longitudinal and transverse components of dielectric permittivity with temperature for pure 6CHBT, composites 1 and 2 showing dielectric anisotropy in the nematic phase at 10 kHz.

Table 3. Longitudinal ($\varepsilon'_{\parallel}$) and Transverse ($\varepsilon'_{\perp}$) Components of the Permittivity, Average Permittivity (ε'_{av}), Dielectric Anisotropy ($\Delta\varepsilon'$), Ratio of the Dielectric Anisotropy and Transverse Component of the Permittivity ($\Delta\varepsilon'/\varepsilon'_{\perp}$) (at 10 kHz), and Relaxation Frequency (f_R) in MHz for Pure 6CHBT NLC and Its Composites with GNRs at 25 °C

	$\varepsilon'_{\parallel}$	$\varepsilon'_{\perp}$	$\varepsilon'_{av} = \frac{(\varepsilon'_{\parallel} + 2\varepsilon'_{\perp})}{3}$	$\Delta\varepsilon' = \varepsilon'_{\parallel} - \varepsilon'_{\perp}$	$\Delta\varepsilon'/\varepsilon'_{\perp}$	f_R (28 °C)
pure 6CHBT	10.8	4.1	6.32	6.7	1.64	3.05
6CHBT + 0.05 wt % GNRs	10.5	4.1	6.20	6.4	1.58	2.20
6CHBT + 0.1 wt % GNRs	10.4	3.6	5.85	6.8	1.93	2.51

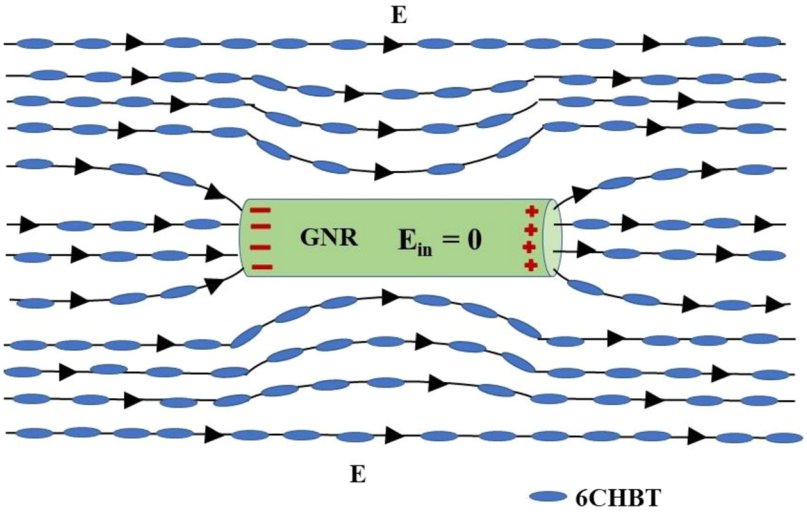

Figure 8. Interaction of LC molecules with GNRs through induced charges in GNRs in the presence of the local electric field of LC molecules. Net electric field inside GNRs is 0. Outside the GNRs, net electric field is indicated by the arrows.

the aromatic ring (δ^{NCS}) or ($\gamma^{(=CH)}$).[38] The value of these peaks for LC-GNR composites is shown in Table 2. As the concentration of GNRs in the LC system is very low, a substantial change is not observed in the peak values. This suggests that the addition of GNRs has not made any changes in the structure of LC molecules. Further, IR spectra for composite 1 and composite 2 do not show any additional peak/peaks (as compared to that of the pure 6CHBT) which may indicate any trace of water or chloroform left in these samples. This shows that water and chloroform were completely removed after drying the samples.

3.4. Dielectric Study. The variations in transverse ($\varepsilon'_{\perp}$) and longitudinal ($\varepsilon'_{\parallel}$) components of the relative permittivity (henceforth, we will call only permittivity for brevity) with respect to temperature are shown in Figure 7 for pure NLC and their composites with GNRs. The permittivity of a material mostly depends upon its structure. With the change in phase, its structure and permittivity change. Therefore, a change in the value of permittivity is observed with the change

https://doi.org/10.1021/acsomega.3c01863
ACS Omega 2023, 8, 29012−29024

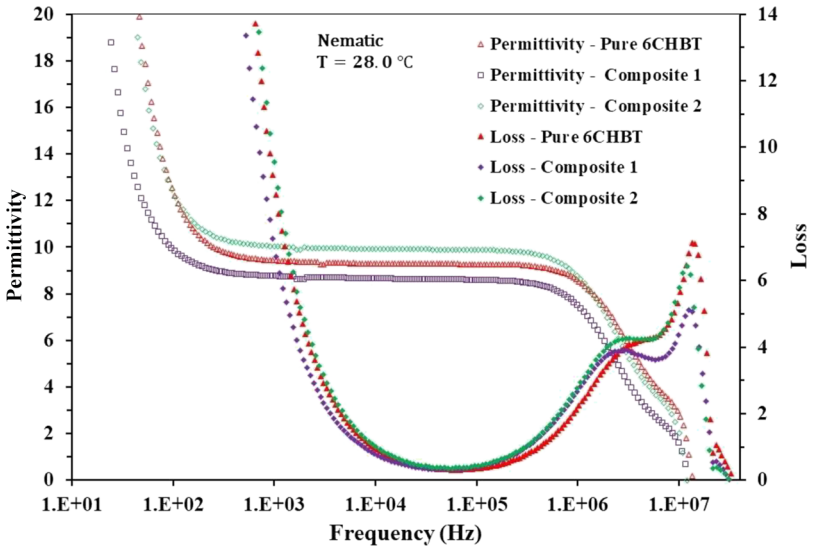

Figure 9. Typical experimental dielectric spectra of permittivity and loss for pure 6CHBT and its composites with GNRs for the homeotropic cells.

of phase.[42] As there is no orientation of molecules in the isotropic phase, the value of both components of permittivity remains the same. However, on decrease of temperature below T_{IN}, it is observed that the molecules try to orient themselves in a planar or homeotropic manner leading to two different values of permittivity as can be seen in Figure 7.

The samples were taken in homeotropic (for measuring $\varepsilon'_{\parallel}$) and planar (for measuring $\varepsilon'_{\perp}$) cells which force the LC molecules to get aligned parallel and perpendicular to the surfaces of the electrodes, respectively, leading to increase in the stability of the mesophase.[24−26,43,44] The dielectric anisotropy is calculated for pure 6CHBT and its two composites with GNRs by using the values of transverse and longitudinal components of permittivity by the following relation $\Delta\varepsilon' = \varepsilon'_{\parallel} - \varepsilon'_{\perp}$. The average permittivity (ε'_{av}) at 25 °C is calculated using the relation $\varepsilon'_{av} = \frac{(\varepsilon'_{\parallel} + 2\varepsilon'_{\perp})}{3}$. The values of transverse and longitudinal components of permittivity and dielectric anisotropy are given in Table 3.

$\varepsilon'_{\parallel}$ and $\varepsilon'_{\perp}$ values for pure 6CHBT match with the literature data.[3,44] For composites 1 and 2, low-frequency parasitic effects have not increased (see Figure 9) as compared to pure 6CHBT. The presence of water and/or chloroform contents highly affects low-frequency dielectric data which have not been observed. It also indicates the absence of undesired water and chloroform contents in composites 1 and 2 as indicated by IR spectra analysis in the previous Section 3.3. Table 3 shows that $\varepsilon'_{\parallel}$ and $\varepsilon'_{\perp}$ are marginally decreasing with increasing concentration of GNRs. $\Delta\varepsilon'$ decreases for composite 1 and then increases for composite 2. GNRs lying in the local electric field of LC molecules form electric dipoles due to the induced charges[45,46] as shown in Figure 8. These induced charges (and hence dipoles) have an electric field opposite to the main electric field of the LC molecules. Induced dipole moment in the GNRs opposite to the dipoles of the LC molecules (as shown in Figure 8) causes a reduction of the permittivity values.

The static dielectric parameters in the nematic phase are governed by Maier and Meier theory.[47] According to this theory, the longitudinal ($\varepsilon'_{\parallel}$) and transverse ($\varepsilon'_{\perp}$) components of relative permittivity in nematic phase are given by the following relation:

$$\varepsilon'_{\parallel} = 1 + \frac{NHF}{\varepsilon_o}\left\{\alpha_{av} + \frac{2}{3}S\Delta\alpha + F\frac{\mu^2}{3kT}[1 - (1 - 3\cos^2\beta)S]\right\} \quad (2)$$

$$\varepsilon'_{\perp} = 1 + \frac{NHF}{\varepsilon_o}\left\{\alpha_{av} - \frac{1}{3}S\Delta\alpha + F\frac{\mu^2}{3kT}\left[1 + \left(\frac{1}{2} - 3\cos^2\beta\right)S\right]\right\} \quad (3)$$

where N is number density of LC molecules, S is the order parameter, $\Delta\alpha$ is the anisotropy of polarisibility, α_{av} is the average polarizability, μ is the resultant dipole moment of the molecule, β is the angle between the dipole moment and long axis of the molecule, F is the feedback factor, and $H = 3\varepsilon'_{av}(0)/(2\varepsilon'_{av}(0) + 1)$.

Subtracting eq 3 from (2) will yield dielectric anisotropy

$$\Delta\varepsilon' = \frac{NHF}{\varepsilon_o}\left[\Delta\alpha - \frac{F}{2kT}\mu^2(1 - 3\cos^2\beta)\right]S \quad (4)$$

According to eq 4, dielectric anisotropy is directly proportional to orientational order parameter S and the number of molecules N. The dielectric strength for pure 6CHBT (6.71) is found to be greater than that for composite 1 (6.40) but smaller than that for composite 2 (6.87). As discussed earlier in the section of calorimetric study, on addition of GNRs, the number density of LC molecule decreases (dilution effect) due to which $\Delta\varepsilon'$ is decreasing for composite 1. However, there is a second factor according to which, with the increase of GNR concentration, the interaction between GNRs and LC molecules increases. Podgornov et al. have also discussed about the interaction of GNRs and LC molecules due to charge transfer complex.[48] According to Shen and Dierking,[49] when LC molecules are dispersed with nanorods or nanotubes, the later get aligned parallel to the nematic director. This results in improvement of local short-range orientational ordering of the molecules. It results in the increase of orientational order parameter (S) of nematic phase which increases the value of $\Delta\varepsilon'$.[50] For composite 2, the

https://doi.org/10.1021/acsomega.3c01863
ACS Omega 2023, 8, 29012−29024

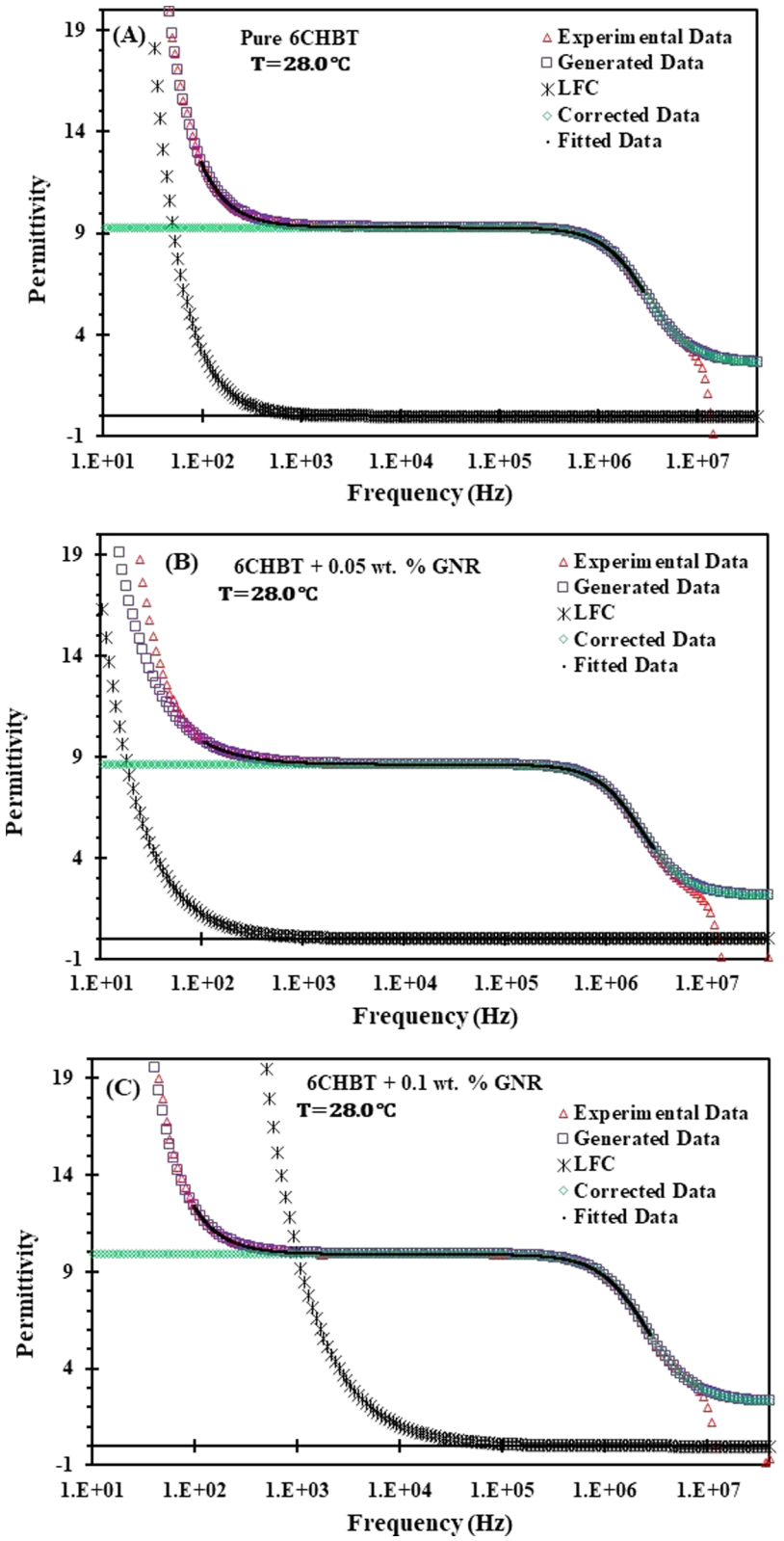

Figure 10. Removal of low- and high-frequency parasitic effects from the experimental dielectric spectra for the permittivity acquired in the nematic phase. Figures (A), (B), and (C) are permittivity for pure 6CHBT, composite 1, and composite 2, respectively. The experimental data are represented with open triangles, whereas the open rhombus show the corrected data. Solid line shows best fit to the experimental data with generalized Cole-Cole equation. Open squares show generated data, whereas stars show low-frequency correction.

second factor dominates over first factor (dilution effect) and hence dielectric anisotropy increases.

Experimental frequency response of permittivity and loss for Pure 6CHBT and composites 1 and 2 are shown in Figure 9 for the homeotropic cells.

https://doi.org/10.1021/acsomega.3c01863
ACS Omega 2023, 8, 29012−29024

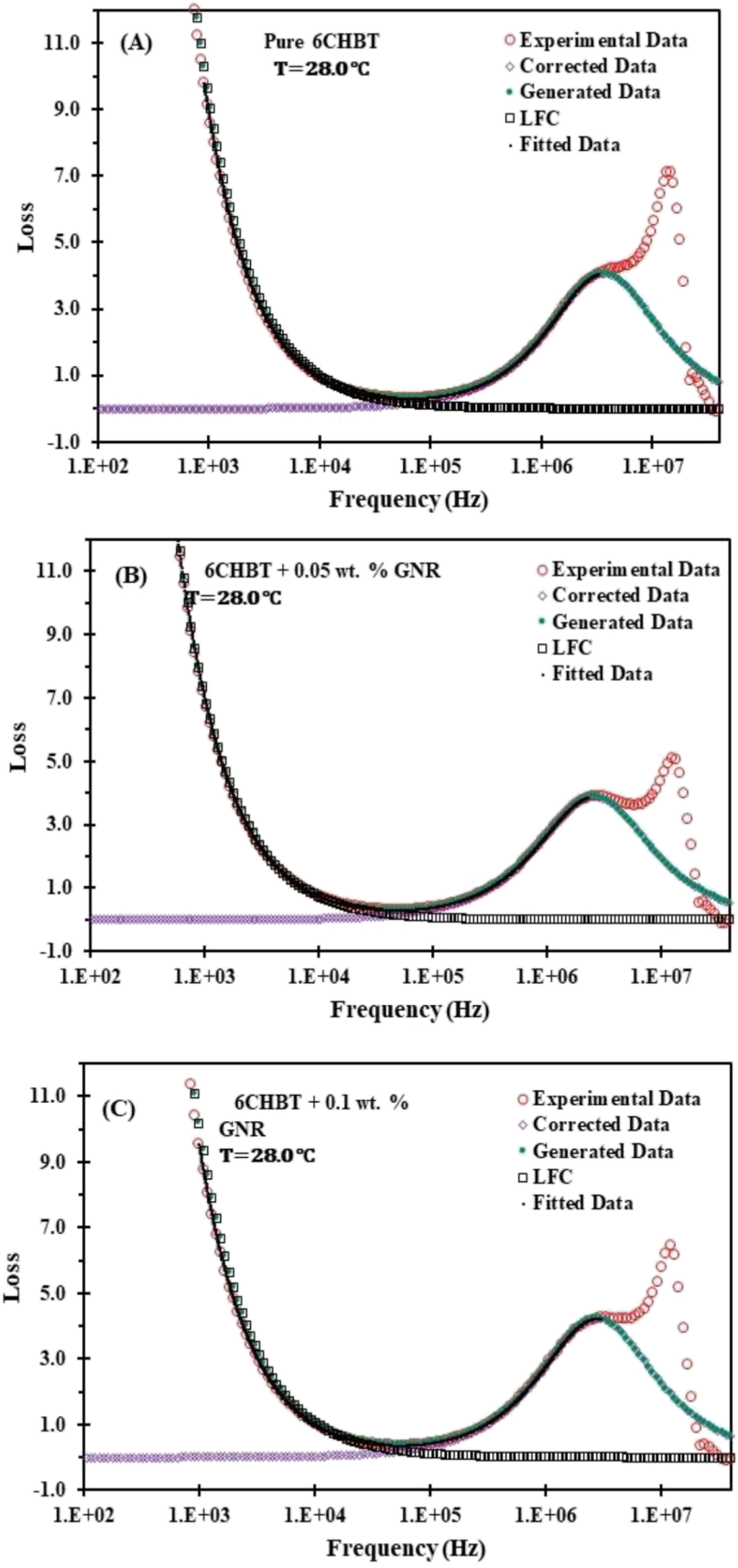

Figure 11. Removal of low- and high-frequency parasitic effects from the experimental dielectric spectra for loss acquired in the nematic phase. Figures (A), (B), and (C) are loss for pure 6CHBT, composite 1, and composite 2, respectively. The experimental data are represented with open circles, whereas the open rhombus show the corrected data. Solid line shows best fit to the experimental data with generalized Cole−Cole equation. Solid circle shows generated data, whereas the open square shows low-frequency correction.

https://doi.org/10.1021/acsomega.3c01863
ACS Omega 2023, 8, 29012−29024

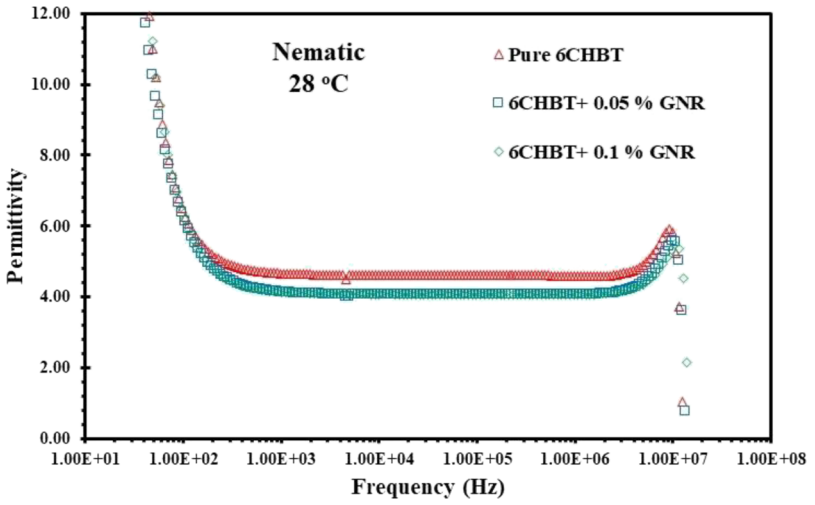

Figure 12. Typical experimental dielectric spectra of the permittivity for pure 6CHBT and two composites with GNRs of different doping concentrations for planar cells.

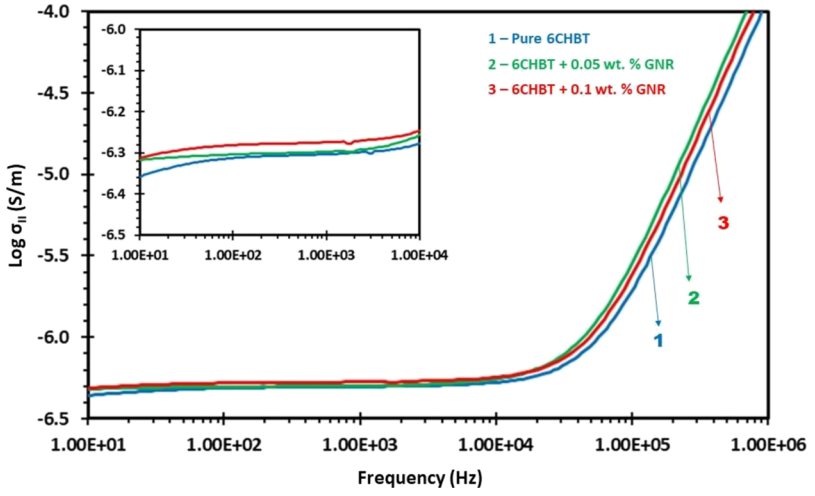

Figure 13. Variation of total conductivity along the long axes of the molecules ($\sigma_{||}$) with a frequency in the nematic phase at 28 °C.

Extraction of the correct frequency response of permittivity and loss after the removal of the low- and high-frequency parasitic effects[45,46] are shown in Figures 10 and 11.

The frequency dependences of permittivity for planar aligned samples are shown in Figure 12.

Figure 12 shows that permittivity measured through the planar aligned samples (transverse component of permittivity, i.e., $\varepsilon'_{\perp}$) is almost constant in the frequency range of 1 kHz−3 MHz which indicate that any molecular relaxation phenomenon for the planar-aligned samples is above 10 MHz. Which is expected, because in the case of planar-aligned samples, the long axes of the molecules are parallel to the cell electrodes. Due to the application of measuring electric field through electrodes, molecules rotate about their long axes and hence they have high relaxation frequency (due to low inertia) as compared to the homeotropic aligned sample where long axes of the molecules are normal to the cell electrodes and they rotate about their short axes (hence high inertia) on the application of the measuring electric field. As expected with the above discussion, a relaxation mode is evident in the homeotropic aligned molecules in the MHz region which is due to the flip-flop motion of LC molecules around their short axes. The relaxation frequency for pure 6CHBT is found to be 3.05 MHz which is decreased to 2.20 MHz for composite 1 and again increased to 2.51 MHz for composite 2. The values of relaxation frequency are governed by two factors, moment of inertia, and viscosity. As the viscosity decreases (dilution effect), relaxation frequency increases, whereas relaxation frequency also decreases with the increase of moment of inertia. Due to the presence of GNRs, viscosity is decreasing but moment of inertia of the system is increasing. In the present case for composite 1, the viscosity effect dominates the inertia effect, whereas for composite 2, the inertia effect dominates the viscosity effect.

The total electrical conductivity (σ) of LC molecules follows the following equation:

$$\sigma = \sigma_i + Cf^m \tag{5}$$

where C is the pre-exponential factor and m is the fractional exponent lying between 0 and 1. σ_i represents the ionic conductivity which is due to the presence of ionic impurities and their conduction on the application of electric field. In the low-frequency region (below 1 kHz), the second dipolar part (Cf^m) is negligible. Hence, in this region, total conductivity is due to only ionic part, $\sigma = \sigma_i$. Figure 13 shows a plot between log of conductivity in (S/m) versus frequency (Hz). It shows

https://doi.org/10.1021/acsomega.3c01863
ACS Omega 2023, 8, 29012−29024

that there is no change in conductivity on addition of GNRs in pure 6CHBT. No change in the conductivity of LC material on addition of any dopant is a favorable condition for display applications.

4. CONCLUSIONS

Infusion of GNRs has not affected the overall morphology of the host nematic liquid crystalline material and hence their mesomorphic behavior. Infusion of GNRs in the matrix of LC molecules is expected to improve the stability of the nematic phase. The two opposing effects suggested by the mean-field theory are responsible for the observed effects in mesomorphic behavior. Initially, transition temperature and enthalpy of N−I transition has decreased due to the decrease in nematic ordering through the dilution effect on addition of GNRs. On the further increase of GNRs concentration, the interaction between GNRs and LC molecules starts to dominate the dilution effect, and therefore, transition temperature and enthalpy of N−I transition (and hence the stability of the nematic phase) show an increasing trend. Due to the low concentration of GNRs in the LC system, no substantial change in the vibrational frequency of pure 6CHBT is observed. This suggests that the addition of GNRs has not affected the structure of LC molecules. An induced dipole is created in GNRs in the local field of LC molecules which forms an antiparallel combination with LC dipoles, and hence, the net dipole moment of the system and consequently permittivity values are decreasing due to the infusion of GNRs. Relaxation frequency corresponding to the rotation of molecules about their short axes is marginally decreasing due to the excess inertia created by GNRs. The ratio of the dielectric anisotropy to the transverse component of the permittivity is an important parameter for displays. This value has decreased for the composite having 0.05% wt % of GNRs which means it will have steep transmission−voltage curve which is beneficial. Unlike most of the other LC-nano-composites where conductivity increases and makes the systems unsuitable for display applications, in the present GNR-LC system, conductivity remains unchanged.

AUTHOR INFORMATION

Corresponding Authors

Abhinav Lal − *Department of Chemistry, Ewing Christian College, University of Allahabad, Prayagraj 211003, India; Centre of Material Sciences, University of Allahabad, Prayagraj 211002, India;* orcid.org/0009-0007-4660-7296; Email: abhinavlal@ecc.ac.in

Ravindra Dhar − *Centre of Material Sciences, University of Allahabad, Prayagraj 211002, India;* orcid.org/0000-0002-4685-6299; Email: rdhar@allduniv.ac.in

Authors

Himanshu Verma − *Centre of Material Sciences, University of Allahabad, Prayagraj 211002, India*

Saikumar Chirra − *Centre of Material Sciences, University of Allahabad, Prayagraj 211002, India; Department of Physics, Ewing Christian College, University of Allahabad, Prayagraj 211003, India*

Roman Dabrowski − *Department of Applied Sciences and Chemistry, Military University of Technology, Warsaw 00-908, Poland*

Kusum Lata Pandey − *Department of Physics, Ewing Christian College, University of Allahabad, Prayagraj 211003, India*

Complete contact information is available at: https://pubs.acs.org/10.1021/acsomega.3c01863

Notes

The authors declare no competing financial interest.

ACKNOWLEDGMENTS

We thank the Department of Science and Technology, Government of India, New Delhi, for financial support to Centre of Materials Sciences, University of Allahabad, Prayagraj under the FIST program under grant No. FST/PSI-216/2016.

REFERENCES

(1) Vafaie, R.; Vahedi, A.; Zakerhamidi, M. S.; Tajalli, H. Dielectric and electro optical properties of 6CHBT nematic liquid crystals doped with MgO nanoparticles. *Liq. Cryst.* **2021**, *48*, 1417−1428.

(2) Sharma, D.; MacDonald, J. C.; Iannacchione, G. S. Thermodynamics of Activated Phase Transitions of 8CB: DSC and MC Calorimetry. *J. Phys. Chem. B* **2006**, *110*, 16679−16684.

(3) Elkhalgi, H. H. M.; Khandka, S.; Singh, U. B.; Pandey, K. L.; Dabrowski, R.; Dhar, R. Dielectric and electro-optical properties of a nematic liquid crystalline material with gold nanoparticles. *Liq. Cryst.* **2018**, *45*, 1795−1801.

(4) Chandrasekhar, S. *Liquid Crystals*; Cambridge University Press: England, 1992.

(5) Wolarz, E.; Bauman, D.; Jadzyn, J.; Dabrowski, R. Prenematic Self-Assembling of Mesogenic Molecules in Isotropic Liquid and Orientational Order in Nematic Phase. *Acta Phys. Pol.* **2011**, *120*, 447−454.

(6) de Gennes, P. G. *The Physics of Liquid Crystals*; Clarendon Press: Oxford, 1995.

(7) Ghassan, A. A.; Mijan, N.; Taufiq-Yap, Y. H. *Nanomaterials: An Overview of Nanorods Synthesis and Optimization*; IntechOpen, 2020.

(8) Qi, H.; Hegmann, T. Liquid crystal−gold nanoparticle composites. *Liquid Cryst. Today* **2011**, *20*, 102−114.

(9) Tripathi, P.; Mishra, M.; Kumar, S.; Dabroski, R.; Dhar, R. Dependence of physical parameters on the size of silver nano particles forming composites with a nematic liquid crystalline material. *J. Mol. Liq.* **2018**, *268*, 403−409.

(10) Rastogi, A.; Hegde, G.; Manohar, T.; Manohar, R. Effect of oil palm leaf-based carbon quantum dot on nematic liquid crystal and its electro-optical effects. *Liq. Cryst.* **2021**, 812−831.

(11) Bubnov, A.; Bobrovsky, A.; Rychetsky, I.; Fekete, L.; Hamplova, V. Self-Assembling Behavior of Smart Nanocomposite System: Ferroelectric Liquid Crystal Confined by Stretched Porous Polyethylene Film. *Nanomaterials* **2020**, *10*, 1498.

(12) Choudhary, A.; Singh, G.; Biradar, A. M. Advances in gold nanoparticle−liquid crystal composites. *Nanoscale* **2014**, *6*, 7743−7756.

(13) Kaur, S.; Singh, S. P.; Biradar, A. M.; Choudhary, A.; Sreenivas, K. Enhanced electro-optical properties in gold nanoparticles doped ferroelectric liquid crystals. *Appl. Phys. Lett.* **2007**, *91*, No. 023120.

(14) Prakash, J.; Khan, S.; Chauhan, S.; Biradar, A. M. Metal oxide-nanoparticles and liquid crystal composites: a review of recent progress. *J. Mol. Liq.* **2020**, *297*, No. 112052.

(15) Tripathi, P. K.; Mishra, A. K.; Manohar, S.; Gupta, S. K.; Manohar, R. Improved dielectric and electro-optical parameters of ZnO nano-particle (8% Cu2+) doped nematic liquid crystal. *J. Mol. Struct.* **2013**, *1035*, 371−377.

(16) Supreet; Singh, G. Recent advances on cadmium free quantum dots-liquid crystal nanocomposites. *Appl. Mater. Today* **2020**, *21*, No. 100840.

https://doi.org/10.1021/acsomega.3c01863
ACS Omega 2023, 8, 29012−29024

(17) Shukla, R. K.; Chaudhary, A.; Bubnov, A.; Hamplova, V.; Raina, K. K. Electrically switchable birefringent self-assembled nano-composites: ferroelectric liquid crystal doped with the multiwall carbon nanotubes. *Liq. Cryst.* **2020**, *47*, 1379−1389.
(18) Vimat, T.; Pandey, S.; Gupta, S. K.; Singh, D. P.; Manohar, R. Enhanced negative dielectric anisotropy and high electrical conductivity of the SWCNT doped nematic liquid crystalline material. *J. Mol. Liq.* **2015**, *204*, 21−26.
(19) Paul, S. N.; Dhar, R.; Verma, R.; Sharma, S.; Dabrowski, R. Change in Dielectric and Electro-Optical Properties of a Nematic Material (6CHBT) Due to the Dispersion of BaTiO3 Nanoparticles. *Mol. Cryst. Liq. Cryst.* **2011**, *545*, 105−111.
(20) Patro, C. K.; Verma, R.; Garg, A.; Dhar, R.; Dabrowski, R. Boost in the thermal stability, ionic conductivity and director relaxation frequency in the composite of liquid crystal and functionalised multi-walled carbon nanotubes. *Liq. Cryst.* **2020**, *48*, 345−360.
(21) Chemingui, M.; Singh, U. B.; Yadav, N.; Dabrowski, R. S.; Dhar, R. Effect of iron oxide (γ-Fe2O3) nanoparticles on the morphological, electro-optical and dielectric properties of a nematic liquid crystalline material. *J. Mol. Liq.* **2020**, *319*, No. 114299.
(22) Mishra, M.; Dabrowski, R.; Dhar, R. Thermodynamical, optical, electrical and electro - optical studies of a room temperature nematic liquid crystal 4-pentyl-4′- cyanobiphenyl dispersed with barium titanate nanoparticles. *J. Mol. Liq.* **2016**, 247−254.
(23) Shaydyuk, Y.; Puchkovska, G.; Goncharuk, A.; Lebovka, N. I. Aggregation of clay platelets in nematic liquid crystal, 5CB: microstructure, electrical conductivity and rheological investigations. *Liq. Cryst.* **2011**, *38*, 155−161.
(24) Singh, D.; Singh, U. B.; Pandey, M. B.; Dabrowski, R.; Dhar, R. Improvement of orientational order and display parameters of liquid crystalline material dispersed with single-wall carbon nanotubes. *Mater. Lett.* **2017**, *216*, 5−7.
(25) Singh, D.; Singh, U. B.; Pandey, M. B.; Dhar, R. Dielectric and electro-optic behaviour of nematic SWCNT nanocomposites under applied bias field. *Liq. Cryst.* **2019**, *46*, 1389−1395.
(26) Singh, D.; Singh, U. B.; Dhar, R.; Dabrowski, R.; Pandey, M. B. Enhancement of electro-optical and dielectric parameters of a room temperature nematic liquid crystalline material by dispersing multi-walled carbon nanotubes. *Liq. Cryst.* **2020**, *48*, 307−312.
(27) Koenig, G. M., Jr.; Ong, R.; Cortes, A. D.; Moreno-Razo, J. A.; de Pablo, J. J.; Abbott, N. L. Single nanoparticle tracking reveals influence of chemical functionality of nanoparticles on local ordering of liquid crystals and nanoparticle diffusion coefficients. *Nano Lett.* **2008**, *8*, 2362−2368.
(28) Mirzaei, J.; Urbanski, M.; Yu, K.; Kitzerow, H. S.; Hegmann, T. Nanocomposites of a nematic liquid crystal doped with magic-sized CdSe quantum dots. *J. Mater. Chem.* **2011**, *21*, 12710−12716.
(29) Pandey, D. K.; Singh, U. B.; Dhar, R.; Dabrowski, R.; Pandey, M. B. Dielectric and electro-optic properties of 6CHBT nematic liquid crystals and silver nanoparticles composites. *Phase Transit.* **2019**, *92*, 931−938.
(30) Juste, J. P.; Santos, I. P.; Marzan, L. M. L.; Mulvaney, P. Gold nanorods: Synthesis, characterization and applications. *Coord. Chem. Rev.* **2005**, *249*, 1870−1901.
(31) Meng, L.; Zhang, J.; Li, H.; Zhao, W.; Zhao, T. Preparation and Progress in Application of Gold Nanorods. *J. Nanomater.* **2019**, 1−11.
(32) Dabrowski, R.; Dziaduszek, J.; Szczucinskl, T. 4−/Trans-4′-n-Alkylcyclohezxyl/ Isothiocyanatobenzenes a New Class of Low-Melting Stable Nematics. *Mol. Cryst. Liq. Cryst.* **1984**, *102*, 155−160.
(33) Gorkunov, M. V.; Osipov, M. A. Mean-field theory of a nematic liquid crystal doped with anisotropic nanoparticles. *Soft Matter* **2011**, *7*, 4348.
(34) Jadzyn, J.; Hellemans, L.; Czechowski, G.; Legrand, C.; Douli, R. Dielectric and viscous properties of 6CHBT in the isotropic and nematic phases. *Liq. Cryst.* **2010**, *27*, 613−619.
(35) Singh, P. K.; Dubey, P.; Dhar, R.; Dabrowski, R. Improvement in the electro-optical and electronic properties of the reduced graphene oxide dispersed in a liquid crystalline material 4′-octyl-4-cyano-biphenyl. *Liq. Cryst.* **2023**, *50*, 476−494.
(36) Mishra, M.; Kumar, S.; Dhar, R. Effect of dispersed colloidal gold nanoparticles on the electrical properties of a columnar discotic liquid crystal. *RSC Adv.* **2014**, *4*, 62404.
(37) Kopcansky, P.; Tomasovicova, N.; Koneracka, M.; Zavisova, V.; Timko, M.; Dzarova, A.; Sprincova, A.; Eber, N.; Csorba, K. F.; Katona, T. T.; Vajda, A.; Jadzyn, J. Structural changes in the 6CHBT liquid crystal doped with spherical, rodlike, and chainlike magnetic particles. *Phys. Rev. E* **2008**, *78*, No. 011702.
(38) Szaleniec, M.; Sobieraj, R. T.; Witko, W. Theoretical Study of 1-(4-hexylcyclohexyl)-4-isothiocyanatobenzene − molecular properties and spectral characteristics. *J. Mol. Model.* **2009**, *15*, 935−943.
(39) Srivastava, J. K.; Singh, R. K.; Dhar, R.; Singh, S. Studies of dispersed liquid crystals in binary mixtures with ionic liquid and their excitation by electric signals. *RSC Adv.* **2015**, *5*, 86291−86302.
(40) Witko, W.; Padol, A. M.; Zielinski, P. M. Multiple melting phenomena in low mass mesogenic compound. *Phase Transitions* **2007**, *80*, 717−724.
(41) Zhao, T.; Li, Z.; Park, K.; Vaia, R. A.; Knappenberger, K. L., Jr. Photoluminescence of single gold nanorods following nonlinear excitation. *J. Chem. Phys.* **2020**, *153*, No. 061101.
(42) Khare, A.; Uttam, R.; Kumar, S.; Dhar, R. Nanocomposite system of a discotic liquid crystal doped with thiol capped gold nanoparticles. *J. Mol. Liq.* **2022**, *366*, No. 120215.
(43) Huang, Y.; Kim, D. H. Dark-field microscopy studies of polarization-dependent plasmonic resonance of single gold nanorods: rainbow nanoparticles. *Nanoscale* **2011**, *3*, 3228.
(44) Verma, R.; Dhar, R.; Rath, M. C.; Sarkar, S. K.; Dabrowski, R. Electron beam irradiation induced changes in the dielectric and electro-optical properties of a room temperature nematic display material 4-(trans-4-n-hexylcyclohexyl)isothiocyanatobenzoate (6CHBT). *J. Phys. Chem. Solids* **2012**, *73*, 288−295.
(45) Jaiswal, M.; Srivastava, G.; Mishra, S.; Singh, P. K.; Dhar, R.; Dabrowski, R. Synthesis and characterization of semiconducting copper oxide nanoparticles and their impact on the physical properties of a nematic liquid crystalline material 4 -pentyl - 4 ′ -cyanobiphenyl. *J. Mol. Liq.* **2023**, No. 122032.
(46) Srivastava, G.; Jaiswal, M.; Singh, P. K.; Iqbal, A.; Dabrowski, R.; Dhar, R. Enhanced stability of the nematic phase of 4 -pentyl −4′ -cyanobiphenyl due to the dispersion of copper nanoparticles. *Liq. Cryst.* **2023**, 1.
(47) Maier, W.; Meier, G. A simple theory of the dielectric properties of homogeneous oriented liquid crystal phases of nematic type. *Z. Naturforsch. A* **1961**, *16*, 262−267.
(48) Podgornov, F. V.; Ryzhkova, A. V.; Hasse, W. Influence of gold nanorods size on electro-optical and dielectric properties of ferroelectric liquid crystals. *Appl. Phys. Lett.* **2010**, *97*, 212903.
(49) Shen, Y.; Dierking, I. Perspectives in Liquid-Crystal-Aided Nanotechnology and Nanoscience: Review. *Appl. Sci.* **2019**, *9*, 2512.
(50) Dhar, R.; Pandey, A. S.; Pandey, M. B.; Kumar, S.; Dabrowski, R. Optimization of the Display Parameters of a Room Temperature Twisted Nematic Display Material by Doping Single-Wall Carbon Nanotubes. *APEX* **2008**, No. 121501.

https://doi.org/10.1021/acsomega.3c01863
ACS Omega 2023, 8, 29012−29024